Structural Engineering and Mechanics, Vol. 39, No. 4 (2011) 579-598 579
DOI: http://dx.doi.org/10.12989/sem.2011.39.4.579

A novel meshfree model for buckling and vibration analysis of rectangular orthotropic plates

Tinh Quoc Bui*[1] and Minh Ngoc Nguyen[2a]

[1]*Chair of Structural Mechanics, Department of Civil Engineering, University of Siegen, Paul-Bonatz-Strasse 9-11, D-57076, Siegen, Germany*
[2]*Department of Civil Engineering, Ruhr University Bochum, Germany*

(Received November 18, 2010, Accepted May 25, 2011)

Abstract. The present work mainly reports a significant development of a novel efficient meshfree method for vibration and buckling analysis of orthotropic plates. The plate theory with orthotropic materials is followed the Kirchhoff's assumption in which the only deflection is field variable and approximated by the moving Kriging interpolation approach, a new technique used for constructing the shape functions. The moving Kriging technique holds the Kronecker delta property, thus it makes the method efficiently in imposing the essential boundary conditions and no special techniques are required. Assessment of numerical results is to accurately illustrate the applicability and the effectiveness of the proposed method in the class of eigenvalue problems.

Keywords: vibration; meshfree; moving Kriging interpolation; orthotropic plate; buckling

1. Introduction

Buckling and vibration solutions for plates are of great importance in many industrial applications, especially in civil engineering, but dealing with these phenomena is in general not an easy task. A large number of studies on vibration and buckling analyses accounted for plate structures by various approaches can easily be found in the literatures. Among approximation numerical methods, the finite element method (FEM) (Zienkiewicz and Taylor 1989) has been widely used for buckling and vibration analyses of plates because of its versatility in describing the complex geometric, physical properties and many others. The plate elements are increasingly used in civil, marine, machines and device in aerospace, mechanical structures, etc. Thus, a thorough consideration of static buckling and vibration modes for such plates is essential to an efficient and reliable design. Exact solutions for the plates, on the other hand, are desirable since they are able to provide more physical feature insight, more accurate and so on. Unfortunately, such analytical solutions are possible only for a very few simple geometric plates and boundary conditions.

Over the past decades, a new class of methods termed meshfree or meshless methods has been introduced and developed (Atluri and Zhu 1998, Belytschko *et al.* 1994, Liu *et al.* 1996, Liu and

*Corresponding author, Ph.D., E-mail: bui-quoc@bauwesen.uni-siegen.de
[a]MSc, Researcher

Gu 2001), in which the entire domain of relevant problem is discretized by a set of scattered nodes in the influence domain regardless of elements. The basic and advanced of theories and numerical applications can be found in several monographs, e.g., see (Li and Liu 2004, Liu 2003). Krysl and Belytschko (1996), for instance, extended the element-free Galerkin (EFG) method to static analysis of thin plates, (Liu and Chen 2001) employed the EFG to further investigation for static and free vibration of thin plates with complicated shapes, (Wang and Wu 2008) developed an efficient Galerkin meshfree method for analyzing shear deformable cylindrical panels, (Sadeghirad *et al.* 2010) presented a meshless equilibrium on line method for linear elasticity. A brief review of various meshfree methods dealing with such plates can also be found in Bui *et al.* (2009). Of course, meshfree methods are not only applicable to analysis of plate structures, they are originally developed for fracture mechanics (Belytschko *et al.* 1994, Matsubara and Yagawa 2009) and extended to a wide range of engineering problems such as penetration into fiber reinforced concrete (James 2010), nonlinear heat transfer (Singh *et al.* 2007) and many other fields.

However, most recent meshfree methods have the same problem of the lack of the Kronecker's delta property and hence leading to the difficulty in imposing the essential boundary conditions. Many efforts have devoted in order to eliminate such drawback e.g., Lagrange multipliers (Belytschko *et al.* 1994), penalty method (Liu 2003), coupling with the FEM (Belyschko *et al.* 1995), etc. Alternatively, (Gu 2003) first introduced a new approach, the moving Kriging interpolation (MK) technique, for constructing the shape functions which possess the delta property correctly. He successfully applied the MK-based meshfree model for solving a simple problem of steady-state heat conduction. Later, further developments of the method have been studied for two-dimensional solid mechanics (Tongsuk and Kanok-Nukulchai 2004a, b) and shells (Sayakoummane and Kanok-Nukulchai 2007), static analysis of thin plates (Bui *et al.* 2009), dynamic of structures and piezoelectric structures (Bui *et al.* 2010a, b), respectively.

Free vibration analysis of orthotropic plates has analyzed by many different authors using various approaches such as an iterative approach (Chen 1998), superelements (Ahmadian and Sherafati Zangened 2002), an approximate method based on Hearmon expression (Biancolini *et al.* 2005), the FEM in 2D and 3D structures (Lok and Cheng 2001), a meshless collocation method with multiquadrics basis functions (Ferreira and Batra 2005, Ferreura *et al.* 2009), a FE code named IDEAS using 20-node brick elements (Batra *et al.* 2004), etc. On the other hand, buckling analysis by different methods can also be found in the literature. For example, (Allman 1975) calculated buckling loads of flat reinforced plates using the triangular finite elements, (Wang 1997) developed a unified Timoshenko beam B-spline Rayleigh-Ritz method, (Wanji and Cheung 1998) presented a refined triangular discrete Kirchhoff plate element and (Liew and Chen 2004) extended the meshfree radial point interpolation method (RPIM) to buckling analysis of Mindlin plates. In a detailed study of comparison between the RPIM and the Kriging interpolation by Dai *et al.* (2003), it is interestingly found although both are derived from different mathematical approaches but the RPIM and Kriging methods yield exactly the same interpolation functions if considered regardless of the mathematical path. Further developments of the RPIM have been studied by Liu's group many different problems, they are not presented here but easily found in the literature.

For further information in the reference review on orthotropic plate vibration and buckling analysis, one can easily find out them in the literature nowadays. Typically, a short review of free vibration of plates can be found in Biancolini *et al.* (2005), a literature review of vibration analysis of thick plates presented by Liew *et al.* (1995), a wide review of the literature up to 1990 for plate vibration is collected by Leissa (1977, 1981, 1987), for buckling of plates and shells (Bank and Yin

1996, Jones 2006) and so on. In addition to the path of the development of meshfree methods for laminated, plates and shells, a very interesting review has recently made by Liew *et al.* (2011) that may also be interested.

The objective of the present work is to extend the MK meshfree method to stability and free vibration analysis of orthotropic plates. Our special attention is to demonstrate its applicability and effectiveness in the class of eigenvalue problems. The superior advantage over the conventional methods e.g., the moving least square method (MLS), is capable of overcoming the difficulty in enforcing the essential boundary conditions without any special techniques, and its realization is similar to the classical FEM. Moreover, subroutines developed for the FEM that can be easily reused and incorporated into the present method. As far as the present authors' knowledge goes, this task has never studied previously once this work is being reported. The structure of the paper forms as follows. Meshfree method for vibration and buckling problem is presented in the next section, in which the moving Kriging shape function, governing equations and the discretization equations of vibration and buckling are derived. Numerical results are illustrated in Section 3 and we shall end with a conclusion.

2. Meshfree formulation for vibration and buckling problems

2.1 Deriving shape function

Basically, the MK interpolation method is similar to the MLS approximation. In order to approximate the distribution functions $u(\mathbf{x}_i)$ within a sub-domain $\Omega_x \subseteq \Omega$, this function can be interpolated based on all nodal values $\mathbf{x}_i$ $(i \in [1, n])$ within the sub-domain, with n being the total number of the nodes in Ω_x. The MK interpolation $u^h(\mathbf{x})$, $\forall \mathbf{x} \in \Omega_x$ is frequently defined as follows (Gu 2003, Bui *et al.* 2009, Tongsuk and Kanok-Nukulchai 2004).

$$\mathbf{u}^h(\mathbf{x}) = [\mathbf{p}^T(\mathbf{x})\mathbf{A} + \mathbf{r}^T(\mathbf{x})\mathbf{B}]\mathbf{u}(\mathbf{x}) \tag{1}$$

or in a shorter form

$$\mathbf{u}^h(\mathbf{x}) = \sum_I^n \phi_I(\mathbf{x}) u_I \tag{2}$$

with $\phi_I(\mathbf{x})$ is the MK shape function and defined by

$$\phi_I(\mathbf{x}) = \sum_j^m p_j(\mathbf{x}) A_{jI} + \sum_k^n r_k(\mathbf{x}) B_{kI} \tag{3}$$

Matrixes **A** and **B** are obtained through

$$\mathbf{A} = (\mathbf{P}^T\mathbf{R}^{-1}\mathbf{P})^{-1}\mathbf{P}^T\mathbf{R}^{-1} \tag{4}$$

$$\mathbf{B} = \mathbf{R}^{-1}(\mathbf{I} - \mathbf{P}\mathbf{A}) \tag{5}$$

where, **I** is an unit matrix and vector $\mathbf{p}(\mathbf{x})$ is the polynomial with m basis functions

$$\mathbf{p}(\mathbf{x}) = \{p_1(\mathbf{x}) \;\; p_2(\mathbf{x}) \;\; \dots \;\; p_m(\mathbf{x})\}^T \tag{6}$$

On the one side, the matrix **P** has size $n \times m$, is collected values of the polynomial basis functions as

$$\mathbf{P} = \begin{bmatrix} p_1(\mathbf{x}_1) & p_2(\mathbf{x}_1) & \dots & p_m(\mathbf{x}_1) \\ p_1(\mathbf{x}_2) & p_2(\mathbf{x}_2) & \dots & p_m(\mathbf{x}_2) \\ \vdots & \vdots & \ddots & \vdots \\ p_1(\mathbf{x}_n) & p_2(\mathbf{x}_n) & \dots & p_m(\mathbf{x}_n) \end{bmatrix} \tag{7}$$

and $\mathbf{r}(\mathbf{x})$ in Eq. (1) is also formed as

$$\mathbf{r}(\mathbf{x}) = \{R(\mathbf{x}_1, \mathbf{x}) \;\; R(\mathbf{x}_2, \mathbf{x}) \;\; \dots \;\; R(\mathbf{x}_n, \mathbf{x})\}^T \tag{8}$$

where $R(\mathbf{x}_i, \mathbf{x}_j)$ is the correlation function between any pair of the n nodes $\mathbf{x}_i$ and $\mathbf{x}_j$, it is denoted belong to the covariance of the field value $u(\mathbf{x})$: $R(\mathbf{x}_i, \mathbf{x}_j) = \mathrm{cov}[u(\mathbf{x}_i)u(\mathbf{x}_j)]$ and $R(\mathbf{x}_i, \mathbf{x}) = \mathrm{cov}[u(\mathbf{x}_i)u(\mathbf{x})]$. The correlation matrix $\mathbf{R}[R(\mathbf{x}_i, \mathbf{x}_j)]_{n\times n}$ is also given in an explicit form as

$$\mathbf{R}[R(\mathbf{x}_i, \mathbf{x}_j)] = \begin{bmatrix} 1 & R(\mathbf{x}_1, \mathbf{x}_2) & \dots & R(\mathbf{x}_1, \mathbf{x}_n) \\ R(\mathbf{x}_2, \mathbf{x}_1) & 1 & \dots & R(\mathbf{x}_2, \mathbf{x}_n) \\ \vdots & \vdots & \ddots & \vdots \\ R(\mathbf{x}_n, \mathbf{x}_1) & R(\mathbf{x}_n, \mathbf{x}_2) & \dots & 1 \end{bmatrix}$$

A concise discussion for the appropriate choice of the correlation function can be found in Gu (2003) and many correlation functions can be employed for **R** but the Gaussian function is often and widely used

$$R(\mathbf{x}_i, \mathbf{x}_j) = e^{-\theta r_{ij}^2} \tag{10}$$

where $r_{ij} = \|\mathbf{x}_i - \mathbf{x}_j\|$, in which $\theta > 0$ is a correlation parameter, which has a certain effect on solution. The quadratic basic $\mathbf{p}^T(\mathbf{x}) = [1 \; x \; y \; x^2 \; y^2 \; xy]$ is employed for computations in this work. The thin plate theory requires not only the first-order derivatives but the second-order derivatives as given below are also handled

$$\phi_{I,i}(\mathbf{x}) = \sum_j^m p_{j,i}(\mathbf{x}) A_{jI} + \sum_k^n r_{k,i}(\mathbf{x}) B_{kI} \tag{11}$$

$$\phi_{I,ii}(\mathbf{x}) = \sum_j^m p_{j,ii}(\mathbf{x}) A_{jI} + \sum_k^n r_{k,ii}(\mathbf{x}) B_{kI} \tag{12}$$

The concept of influence domain where an influence domain radius is defined to determine the number of scattered nodes within an interpolated domain of interest. In this work, the following relation is taken to compute the size of support domain

$$d_m = \alpha d_c \tag{13}$$

where d_c being a characteristic length relative to the nodal spacing close to the point of interst while α stands for a scaling factor. Note that other desirable properties of the MK method i.e., the Kronecker delta functions and consistency properties, are not repeated here because of keeping the manuscript as concise as possible but can be easily found in the above-mentioned references.

Noted also, the Gaussian correlation function above is sensitive to the correlation parameter whose value is found to be unrelated to any physical aspect of the problem. In practice, deriving optimal values of the correlation parameter for all problems is very difficult. It varies from one to another problem and in theory no exact rules to get such a single optimal value for all problems. Hence, it is of interest to alternatively evaluate of the correlation parameter so that there should be existed an acceptable range on its magnitude to ensure consistency in the quality of the results.

2.2 Governing equations for orthotropic plates

In this section, our attention will be focused on a brief representation of stress-strain relationship, elastic constants and dynamic equation for orthotropic plate in a plane stress statement. As can be known that, an orthotropic material is generally characterized by the fact that the mechanical elastic properties have two perpendicular planes of symmetry. Due to this condition, only four elastic constants such as $E_1, E_2, G_{12}, \nu_{12}$ are independent. Additionally, the quantity ν_{21} can also be determined using the following relation

$$\frac{\nu_{12}}{\nu_{21}} = \frac{E_1}{E_2} \tag{14}$$

Now let us consider a plate as shown in Fig. 1 under the Cartesian coordinate system, the displacements of the plate in the *x*, *y*, *z* directions are denoted by u, v, w, respectively. In meshfree methods, the plate is represented by a set of nodes scattered in the relevant plate domain. The deflection $w(\mathbf{x})$ with $\mathbf{x} = \{x, y\}^T$ is directly approximated using parameters of nodal deflection w_I expressed in a form as

$$w^h(\mathbf{x}) = \sum_I^n \phi_I(\mathbf{x}) w_I \tag{15}$$

where the $\phi_I(\mathbf{x})$ are the meshfree MK shape functions given in Eq. (3). According to (Liu 2003, Vinson 2005), the equation of the motion of a orthotropic plate including the in-plane loads and neglecting the shear effect in a strong form can be explicitly represented in a fourth-order equation

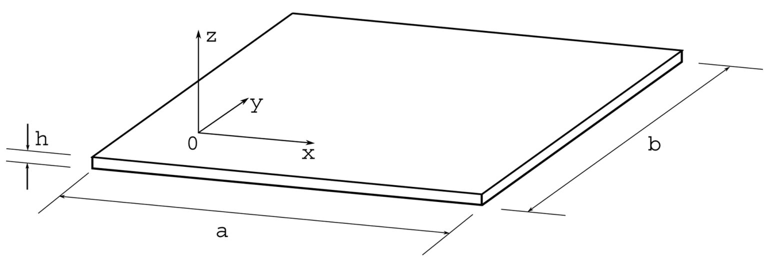

Fig. 1 The geometry of a plate and its parameters

as

$$D_{11}\frac{\partial^4 w}{\partial x^4}+2(D_{12}+2D_{66})\frac{\partial^4 w}{\partial x^2\partial y^2}+D_{22}\frac{\partial^4 w}{\partial y^4}+\rho h\ddot{w} = N_x\frac{\partial^2 w}{\partial x^2}+2N_{xy}\frac{\partial^2 w}{\partial x\partial y}+N_y\frac{\partial^2 w}{\partial y^2} \tag{16}$$

with ρ and h stand for the mass density of the material and the thickness of the plate, other flexural rigidity quantities are given as follows

$$D_{11} = \frac{E_1 h^3}{12(1-\nu_{12}\nu_{21})};\quad D_{12} = \frac{E_2 h^3 \nu_{12}}{12(1-\nu_{12}\nu_{21})};\quad D_{22} = \frac{E_2 h^3}{12(1-\nu_{12}\nu_{21})};\quad D_{66} = \frac{G_{12}h^3}{12} \tag{17}$$

and the components of in-plane forces acting on the plate on its edges as

$$\mathbf{N} = \{N_x\ \ N_y\ \ N_{xy}\}^T \text{ and } N_x = -N_0;\ \ N_y = -\mu_1 N_0;\ \ N_{xy} = -\mu_2 N_0 \tag{18}$$

where N_0 is a constant and μ_1; μ_2 are possibly functions of coordinates (Liu 2003). Based on the assumption of classical thin plate, the displacement fields can be defined as

$$\mathbf{u} = \{u\ \ v\ \ w\}^T = \left\{-z\frac{\partial w}{\partial x}\ \ -z\frac{\partial w}{\partial y}\ \ w\right\}^T = \hat{\mathbf{L}}w \tag{19}$$

The strains and stresses of the plate are obtained by

$$\boldsymbol{\varepsilon}_p = \left\{-\frac{\partial^2 w}{\partial x^2}\ \ -\frac{\partial^2 w}{\partial y^2}\ \ -2\frac{\partial^2 w}{\partial x\partial y}\right\}^T = \mathbf{L}w \tag{20}$$

$$\boldsymbol{\sigma}_p = \{M_x\ \ M_y\ \ M_{xy}\}^T \tag{21}$$

where M_x, M_y and M_{xy} in Eq. (21) are bending and twisting moments, respectively. The constitutive equation of the relationship between the strain and stress can be thus expressed as

$$\boldsymbol{\sigma}_p = \mathbf{D}\boldsymbol{\varepsilon}_p \tag{22}$$

where $\mathbf{D}$ are the matrix of constant related to the material property and thickness of the plate, $\boldsymbol{\sigma}_p$ and $\boldsymbol{\varepsilon}_p$ are defined as pseudo-strains and –stresses. For an orthotropic plate, they simply have

$$\mathbf{D} = \begin{bmatrix} D_{11} & D_{12} & 0 \\ D_{12} & D_{22} & 0 \\ 0 & 0 & D_{66} \end{bmatrix} \tag{23}$$

By following the classical plate assumption, it is noted that the only the deflection $w(\mathbf{x})$ is an independent variable and approximated by the MK method. The other two displacement components $u(\mathbf{x})$ and $v(\mathbf{x})$ are extracted directly from the deflection $w(\mathbf{x})$ through the relation given in Eq. (19).

2.3 Discrete equations

To derive the dynamic equations for free vibration and for buckling of the plate, the Lagrangian equation is employed (Liu 2003)

$$\frac{d}{dt}\left\{\frac{\partial \Xi}{\partial \dot{w}}\right\} - \left\{\frac{\partial \Xi}{\partial w}\right\} = 0 \tag{24}$$

where $\Xi = T - \Pi$ is known as the Lagrangian functions with T is the kinetic energy of the system, $\Pi = \Pi_b + \Pi_i$ being the strain energy of bending Π_b and strain energy caused by in-plane forces Π_i of the plate, respectively. The kinetic energy of the system is expressed as

$$T = \frac{1}{2}\int_{\Omega} \rho \dot{\mathbf{u}}^T \dot{\mathbf{u}} d\Omega \tag{25}$$

The total potential energy of the plate including the strain energies caused by bending and by in-plane forces of the plate that can be written as

$$\Pi = \Pi_b + \Pi_i = \frac{1}{2}\int_{\Omega} \boldsymbol{\varepsilon}_p^T \boldsymbol{\sigma}_p d\Omega - \int_{\Gamma_\sigma} \mathbf{u}^T \bar{\mathbf{t}} d\Gamma - \int_{\Omega} \mathbf{u}^T \bar{\mathbf{b}} d\Omega + \frac{1}{2}\int_{\Omega} \boldsymbol{\varepsilon}_p^T \mathbf{N} d\Omega \tag{26}$$

where $\bar{\mathbf{t}}$ and $\bar{\mathbf{b}}$ denote prescribed boundary forces and a body force vector, respectively. Substituting Eqs. (25) and (26) into Eq. (24) employed simultaneously other Eqs. (18)-(22), we derived the weak form of the dynamic equations of the system as

$$\begin{aligned} &\frac{d}{dt}\int_{\Omega} \rho \frac{\partial}{\partial \dot{w}} (\hat{\mathbf{L}}\dot{w})^T (\mathbf{L}\dot{w}) d\Omega + \int_{\Omega} \frac{\partial}{\partial w} (\mathbf{L}w)^T \mathbf{D} (\mathbf{L}w) d\Omega + \int_{\Omega} \frac{\partial}{\partial w} (\mathbf{L}w)^T \mathbf{N} d\Omega \\ &= \int_{\Gamma_\sigma} \frac{\partial}{\partial w} (\hat{\mathbf{L}}\dot{w})^T \bar{\mathbf{t}} d\Gamma + \int_{\Omega} \frac{\partial}{\partial w} (\mathbf{L}w)^T \bar{\mathbf{b}} d\Omega \end{aligned} \tag{27}$$

However, since free of external forces is taken into account for the vibration and buckling analyses of the plate, the terms on the right-hand-side is omitted in this study.

2.3 Free vibration analysis

On substituting the deflection field w of the form as shown in Eq. (15) into the variational form handled in Eq. (27) neglecting the last term of the in-plane forces, the final undamped dynamic discrete equation for free vibration analyses can be given by

$$\mathbf{M}\ddot{\mathbf{w}} + \mathbf{K}\mathbf{w} = 0 \tag{28}$$

where $\mathbf{w}, \mathbf{K}$ and $\mathbf{M}$ stand for the vector of general nodal deflections, global stiffness and mass matrices, respectively, and they have a form as

$$K_{IJ} = \int_{\Omega} \mathbf{B}_I^T \mathbf{D} \mathbf{B}_J d\Omega \tag{29}$$

$$M_{IJ} = \int_{\Omega} (\rho \phi_I \phi_J h + \phi_{I,x} \phi_{J,x} I + \phi_{I,y} \phi_{J,y} I) d\Omega \tag{30}$$

$$\mathbf{B}_I = \{-\phi_{I,xx} \ \ -\phi_{I,yy} \ \ -2\phi_{I,xy}\}^T \tag{31}$$

where $I = \rho(h^3/12)$ is the mass moment of inertial. As a consequence, a general solution of such a homogeneous equation can be written as

$$\mathbf{w} = \overline{\mathbf{w}}\exp(i\omega t) \tag{32}$$

where i is the imaginary unit, t indicates time, $\overline{\mathbf{w}}$ is the eigenvector and ω is natural frequency. Inserting the general solution given in Eq. (32) into Eq. (28), the natural frequency ω of the vibration of plate can be gained by solving the following eigenvalue equation

$$(\mathbf{K} - \omega^2\mathbf{M})\overline{\mathbf{w}} = 0 \tag{33}$$

2.4 Buckling analysis

Likewise, also on substituting the deflection field^w of the form given in Eq. (15) into the variational form shown in Eq. (27) neglecting the effect of the kinetic energy presented within the first term. We obtain the discrete equation for buckling analysis of the plate as follows

$$(\mathbf{K} - N_0\mathbf{G})\mathbf{w} = 0 \tag{34}$$

with $\mathbf{K}$ is the stiffness matrix shown in Eq. (29) above, N_0 is the eigenvalue for a unitary compressive load or critical buckling loads which is needs to be determined, and $\mathbf{G}$ expresses the geometric stiffness matrix by

$$G_{IJ} = \int_{\Omega} \phi_{I,x}\phi_{J,x} + \mu_1\phi_{I,y}\phi_{J,y} + \mu_2(\phi_{I,x}\phi_{J,y} + \phi_{J,x}\phi_{I,y})d\Omega \tag{35}$$

By solving Eq. (34) we can obtain the critical buckling loads of the orthotropic plate that subjected to the in-plane loads. Here we use a background cell of 16 Gaussian points for the purpose of numerical integration of the stiffness and mass matrices.

3. Numerical analysis

To illustrate the applicability of the proposed method to eigenvalue analysis of orthotropic plate, various geometric shapes of plates are considered. The accuracy of the results obtained by the present method is verified by comparing with other approaches available in the literature. For free vibration analysis, the dimensionless natural frequency coefficient $\xi = (\omega^2\rho h a^4/D_3)^{1/4}$ (Liu 2003, Chen *et al.* 2003) with $D_3 = D_{12} + 2D_{66}$, is used, whereas $k = N_0 b^2/\pi^2 D_3$ is used for the buckling analysis if not specified, otherwise. The effectiveness of the method is also studied by using both regularly and irregularly nodal distributions. Only the complete free and simply supported boundary conditions are considered throughout the paper.

It is necessary to point out here that in order to treat the fully clamped boundary for such a thin plate, the boundary conditions with derivatives, i.e., two rotations in this case, must be defined as unknown field variable evolved in the approximation function. However, these derivatives can not be imposed directly because no information of such derivatives is involved in the MK approximation functions. In order to deal with this difficulty, (Li *et al.* 2006) recently introduced an efficient Hermite-type technique incorporated into the RPIM, in which both deflection and its derivatives are involved in the interpolation functions. Another possible strategy proposed by Cui *et al.* (2009), who have introduced a thin plate formulation without rotation DOFs in incorporation various smoothing strain techniques (Chen *et al.* 2001) into the RPIM. The MK method may have a similar manner and in principle, it therefore needs such a development to treat the fully clamped boundary condition. However, this task is in general more challenging and beyond the scope of the present work.

3.1 Free vibration analysis

A rectangular plate depicted in Fig. 1 is first considered. The edges denoted by a, b; the thickness h = 0.05 m and the mass density ρ = 8000 kg/m^3 are used. For the purpose of comparison, the elastic constants are assumed to be similar to those in (Liu 2003, Chen 1998, Chen *et al.* 2003) for the following two cases: (a) if $E_1 \geq E_2$, we choose ν_{12} = 0.3; $\nu_{21} = \nu_{12}E_2/E_1$ and (b) if $E_1 \leq E_2$, then ν_{21} = 0.3; $\nu_{12} = \nu_{21}E_1/E_2$ are chosen.

3.1.1 Simply supported square orthotropic plates

A square plate $a = b = 10$ m is used in the analysis. A regular pattern of 13×13 nodal distribution is considered for all the computations. Based on the previous experience, a correlation parameter $\theta = 5$ and a scaling factor $\alpha = 2.5$ are specified. The natural frequency coefficient ξ is calculated and presented in Table 1 for three different types of the given ratio of flexural rigidity quantities, i.e., D_{22}/D_3 and D_{11}/D_3. As shown in the table, an excellent agreement between two approaches is observed. Additionally, the first twenty eigenmodes of this square orthotropic plate are given in Fig. 2 to have a better view. Noted that Fig. 2 is taken from the case of D_{22}/D_3 = D_{11}/D_3 = 0.5 and the numerical values in brackets in that figure are generally not important because all the solutions have been normalized into a dimensionless coefficient. Nevertheless, these values mean natural frequencies (not normalized) computed by the proposed method.

Table 1 The dimensionless frequency for a fully simply supported orthotropic plate

Mode	$D_{22}/D_3 = 0.5$					
	$D_{11}/D_3 = 0.5$		$D_{11}/D_3 = 1.0$		$D_{11}/D_3 = 2.0$	
	EFG [34]	Present	EFG [34]	Present	EFG [34]	Present
ξ_1	4.130	4.101	4.295	4.283	4.576	4.571
ξ_2	6.333	6.325	6.387	6.397	6.479	6.486
ξ_3	6.341	6.325	6.996	6.989	7.936	7.948
ξ_4	8.273	8.250	8.600	8.635	8.781	8.803
ξ_5	8.714	8.749	8.743	8.777	9.159	9.186
ξ_6	8.732	8.785	9.949	10.007	10.903	11.039
ξ_7	10.411	10.428	10.587	10.594	11.277	11.349
ξ_8	10.422	10.487	11.205	11.222	11.552	11.558
ξ_9	11.242	11.236	11.295	11.269	12.416	12.517
ξ_{10}	11.249	11.232	12.891	12.875	13.515	13.696
ξ_1 [18]	4.118		4.279		4.557	

Table 1 Continued

Mode	$D_{22}/D_3 = 1.0$					
	$D_{11}/D_3 = 0.5$		$D_{11}/D_3 = 1.0$		$D_{11}/D_3 = 2.0$	
	EFG [34]	Present	EFG [34]	Present	EFG [34]	Present
ξ_1	4.295	4.283	4.443	4.446	4.700	4.704
ξ_2	6.387	6.380	7.031	7.076	7.104	7.126
ξ_3	6.996	6.985	7.036	7.076	7.961	7.951
ξ_4	8.600	8.619	8.892	8.921	9.404	9.411
ξ_5	8.743	8.761	9.959	10.059	9.988	10.049
ξ_6	9.949	9.950	9.966	10.098	11.560	11.577
ξ_7	10.587	10.615	11.341	11.364	11.604	11.701
ξ_8	11.205	11.283	11.347	11.376	12.518	12.673
ξ_9	11.259	11.294	13.032	13.251	13.048	13.217
ξ_{10}	12.891	12.889	13.036	13.267	14.110	14.110
ξ_1 [18]	4.279		4.425		4.678	
Mode	$D_{22}/D_3 = 2.0$					
	$D_{11}/D_3 = 0.5$		$D_{11}/D_3 = 1.0$		$D_{11}/D_3 = 2.0$	
	EFG [34]	Present	EFG [34]	Present	EFG [34]	Present
ξ_1	4.576	4.574	4.700	4.703	4.921	4.926
ξ_2	6.479	6.475	7.104	7.159	8.008	8.062
ξ_3	7.936	7.951	7.961	7.973	8.011	8.062
ξ_4	8.781	8.802	9.404	9.446	9.843	9.846
ξ_5	9.159	9.194	9.988	10.043	11.575	11.576
ξ_6	10.903	11.072	11.560	11.618	11.578	11.590
ξ_7	11.277	11.383	11.604	11.618	12.713	12.748
ξ_8	11.552	11.617	12.518	12.592	12.714	12.748
ξ_9	12.416	12.495	13.048	13.205	14.775	14.797
ξ_{10}	13.515	13.529	14.110	14.184	15.285	15.305
ξ_1 [18]	4.557		4.678		4.897	

3.1.2 Natural frequency convergence

Natural frequency coefficients are calculated for a completely simply supported square orthotropic plate corresponding to different densities of regularly distributed nodes. Here, $D_{11}/D_3 = 0.5$ and $D_{22}/D_3 = 0.5$ are considered while $\theta = 2.0$ and $\alpha = 2.5$ are specified. Table 2 shows the results of the frequency parameters versus six different nodal distributions and a good convergence for the proposed method is found.

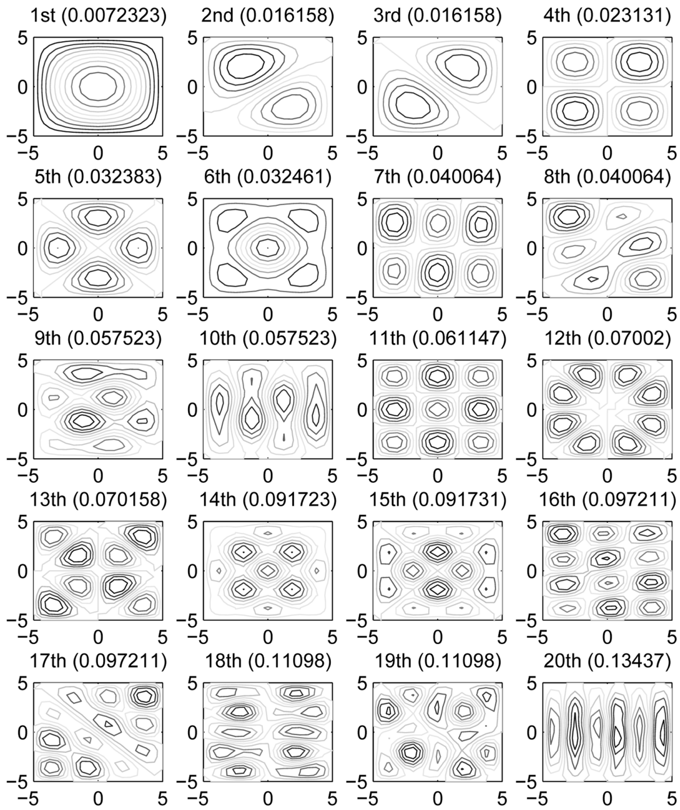

Fig. 2 The first twenty eigenmodes of natural frequency for a fully simply supported square orthotropic plate

Table 2 Convergence of frequency coefficients of a fully simply supported square orthotropic plate

Mode	5×5	9×9	13×13	15×15	17×17	21×21
ξ_1	4.379	4.011	4.023	4.048	4.060	4.070
ξ_2	8.362	6.245	6.091	6.140	6.159	6.150
ξ_3	8.362	6.245	6.091	6.140	6.159	6.168
ξ_4	11.811	7.983	7.582	7.704	7.756	7.762
ξ_5	14.806	9.066	8.469	8.505	8.508	8.550

3.1.3 Effectiveness of irregularly distributed nodes

The nodal distribution in irregular setting is employed to verify the effectiveness of the proposed method. Fig. 3 shows the nodal distributions of regular and irregular systems of a fully simply supported square plate. The ratios of $D_{22}/D_3 = 0.5$ and $D_{11}/D_3 = 0.5$; 1.0 and 2.0, respectively, are typically considered for this purpose. A correlation parameter $\theta = 0.5$ and a scaling factor $\alpha = 2.5$ are taken. The gained results of the first ten frequency coefficients are presented in Table 3 and very good agreements with each other are observed. It probably confirms that no effects of the irregularly on the frequency significantly or implies that no significant variation on nodal density across the domain problem.

Table 3 Comparison of the dimensionless frequency coefficients derived from both regular and irregular distributed nodes for a fully simply supported orthotropic plate

Mode	$D_{22}/D_3 = 0.5$					
	$D_{11}/D_3 = 0.5$		$D_{11}/D_3 = 1.0$		$D_{11}/D_3 = 2.0$	
	Regular	Irregular	Regular	Irregular	Regular	Irregular
ξ_1	4.120	4.172	4.273	4.260	4.567	4.543
ξ_2	6.315	6.290	6.409	6.399	6.586	6.543
ξ_3	6.315	6.301	6.989	6.937	7.948	7.840
ξ_4	8.150	8.108	8.535	8.475	9.103	9.013
ξ_5	8.849	8.942	8.905	9.088	9.186	9.247
ξ_6	8.885	8.986	10.107	10.100	11.239	11.135
ξ_7	10.388	10.334	10.694	10.716	11.749	11.597
ξ_8	10.388	10.500	11.222	11.218	11.858	12.197
ξ_9	11.716	11.459	11.769	11.996	12.517	12.381
ξ_{10}	11.716	11.937	13.055	12.948	13.696	13.699
ξ_1 [18]	4.118		4.279		4.557	

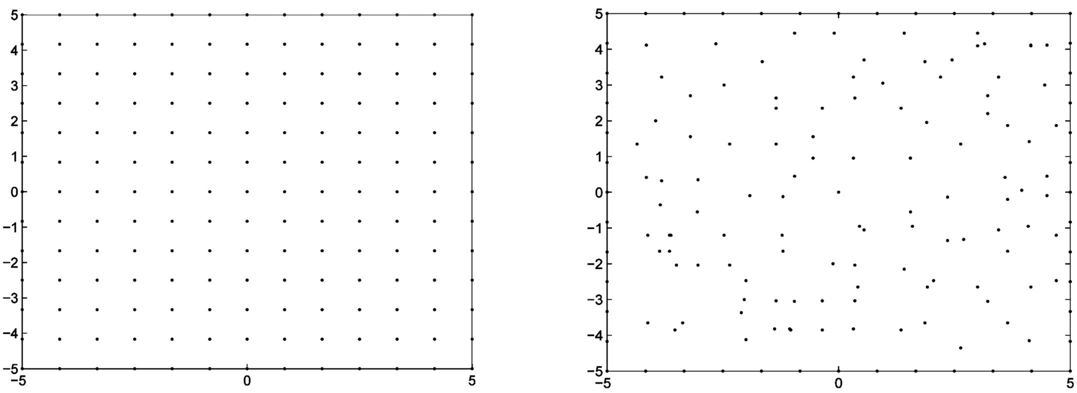

Fig. 3 A square orthotropic plate with 13×13 regular (left) and 169 irregular (right) nodes

3.1.4 Influence of scaling and correlation coefficients

The influence of the scaling factor and the correlation parameter is studied here. The ratios of $D_{11}/D_3 = 0.5$ and of $D_{22}/D_3 = 0.5$ are considered with a 13 × 13 pattern of nodal distribution. For the correlation parameter, it is varied in a wide range for a fixed scaling factor $\alpha = 2.5$, and whereas the scaling factor is varied for a fixed correlation parameter $\theta = 0.5$ for the effect of the scaling factor. The computed results of the frequency coefficients for these two cases are presented in Figs. 4(a) and 4(b), respectively, and found any value taken within these ranges $0.1 \le \theta \le 10$ and $2.5 \le \alpha \le 3.2$ can yield acceptable solutions.

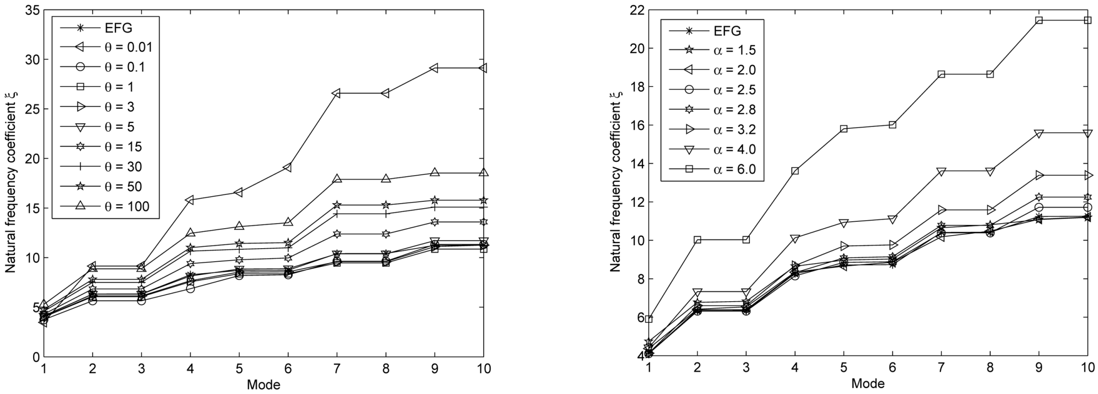

Fig. 4 Variation of the dimensionless frequencies versus the correlation parameter (left) and the scaling factor (right) for a fully simply supported square orthotropic plate

Table 4 Evaluation of the dimensionless frequency coefficients for a completely free square orthotropic plate ($\theta = 5$; $\alpha = 2.5$)

Mode	$D_{22}/D_3 = 0.5$					
	$D_{11}/D_3 = 0.5$		$D_{11}/D_3 = 1.0$		$D_{11}/D_3 = 2.0$	
	Regular	Irregular	Regular	Irregular	Regular	Irregular
ξ_4	3.743	3.755	3.828	3.815	3.853	3.840
ξ_5	3.801	3.786	3.948	3.980	3.989	4.042
ξ_6	4.179	4.209	4.766	4.769	5.648	5.629
ξ_7	5.700	5.768	5.773	5.758	5.870	5.850
ξ_8	5.700	5.718	6.026	6.034	6.513	6.534
ξ_9	6.748	6.795	6.787	6.795	6.859	6.883
ξ_{10}	6.748	6.786	7.864	7.873	8.070	8.179

3.1.5 Completely free boundary conditions

The solutions derived from applying the completely free boundary condition to the orthotropic plates are also provided. The regular and irregular nodal distributions are again considered. The computed results of the natural frequency coefficient $\xi = (\omega^2 \rho h a^4/D_3)^{1/4}$ are presented in Table 4. However, the first three modes that are corresponding to the rigid displacements are hence not listed in the table.

3.1.6 Natural frequency coefficients on the ratio: b/a

As depicted in Fig. 1 above, a and b are specified as its edges length. We here wanted to have a study on the influence of the shape of the plates on the solutions. Five different types of the ratio are calculated for the frequency coefficients and the corresponding results are stored in Table 5 in comparison with those computed by the finite difference method (Chen 1998). As expected, a good agreement with each other is again obtained.

Table 5 Comparison of the calculated frequency coefficients versus various ratios of D_{11}/D_3 for a fully simply supported orthotropic plate with ratios of b/a

b/a	Method	D_{22}/D_3 : 0.5			D_{22}/D_3 : 1.0			D_{22}/D_3 : 2.0		
		D_{11}/D_3			D_{11}/D_3			D_{11}/D_3		
		0.5	1.0	2.0	0.5	1.0	2.0	0.5	1.0	2.0
2.5	(Chen 1998)	2.989	3.362	3.867	3.000	3.370	3.872	3.023	3.386	3.882
	MK	2.970	3.357	3.873	3.053	3.377	3.883	3.032	3.380	3.887
1.5	(Chen 1998)	3.455	3.715	4.113	3.511	3.760	4.147	3.616	3.846	4.212
	MK	3.467	3.743	4.152	3.560	3.797	4.273	3.628	3.899	4.262
1	(Chen 1998)	4.118	4.279	4.557	4.279	4.425	4.678	4.557	4.678	4.897
	MK	4.121	4.289	4.575	4.249	4.430	4.655	4.558	4.686	4.904
2/3	(Chen 1998)	5.183	5.263	5.424	5.572	5.640	5.769	6.170	6.220	6.318
	MK	5.157	5.267	5.477	5.534	5.663	5.777	6.209	6.311	6.358
0.4	(Chen 1998)	7.472	7.501	7.557	8.404	8.424	8.464	9.667	9.680	9.706
	MK	7.470	7.548	7.550	8.417	8.425	8.474	9.654	9.679	9.724

3.2 Buckling analysis

In this section, a fully simply supported orthotropic plate is now employed to appealingly assess at the static buckling loads. Material parameters are the same as above. The standard EFG is used for the same simulation for the purpose of comparison. Only an in-plane compressive load applied in the x direction is considered and this implies that only N_x is valid whereas the others are omitted. The critical buckling factor $k = N_0 b^2/\pi^2 D_3$ is calculated and the results derived from the present method are then compared with that calculated by the EFG. The computed results of the critical buckling factor against various nodal densities are listed in Table 6, in which three different ratios of a/b are considered, respectively. A very good agreement with each other for buckling analysis is found. It can also be observed that the EFG probably has a faster convergence compared with the present method under a course density. Nevertheless, both have a very good convergence when a pattern of 169 nodes is reached. Tables 7 and 8, respectively, show the critical buckling factors calculated for various flexural rigidity ratios of D_{11}/D_3 and correlation parameter, respectively. This

Table 6 Convergence of critical buckling factor $k = N_0 b^2/\pi^2 D_3$ of a fully simply supported square orthotropic plate versus the nodal densities ($D_{22}/D_3 = D_{11}/D_3 = 0.5$, $\alpha = 3$; $\theta = 3$)

Approach	a/b	5×5	9×9	13×13	15×15	17×17	21×21
EFG	1.5	3.472	3.221	3.207	3.195	3.185	3.180
Present		28.053	5.477	3.923	3.192	3.197	3.182
EFG	1.0	3.079	3.012	3.009	3.008	3.004	3.000
Present		24.718	3.581	3.193	3.016	3.002	3.001
EFG	0.5	5.117	4.153	4.137	4.135	4.131	4.127
Present		10.218	4.365	4.173	4.150	4.135	4.130

Table 7 Comparison of the critical buckling factor $k = N_0 b^2/\pi^2 D_3$ of a simply supported orthotropic plate corresponding to various ratios of D_{11}/D_3 accounted for different ratios of *a/b* ($\alpha = 3$; $\theta = 3$; 17×17 nodes)

a/b	$D_{22}/D_{11} = 0.5$					
	$D_{11}/D_3 = 0.5$		$D_{11}/D_3 = 1.0$		$D_{11}/D_3 = 2.0$	
	EFG	Present	EFG	Present	EFG	Present
1.5	3.180	3.182	3.576	3.545	4.021	4.108
1.2	3.068	3.091	3.416	3.426	4.112	4.111
1.0	3.000	3.001	3.501	3.523	4.502	4.528
0.8	3.105	3.169	3.888	3.873	5.454	5.464
0.5	4.127	4.130	6.129	6.128	10.124	10.135

Table 8 Evaluation of critical buckling factor against different specified correlation parameters corresponding to various ratios of *a/b* for an orthotropic plate ($D_{22}/D_3 = D_{11}/D_2 = 0.5$, $\alpha = 3$ is fixed, 17×17 nodes)

a/b	$\theta = 0.1$	$\theta = 1$	$\theta = 3$	$\theta = 5$	$\theta = 7$	$\theta = 10$	$\theta = 20$	$\theta = 50$	EFG
1.5	1.604	3.340	3.182	3.177	3.182	3.428	7.436	10.391	3.180
1.2	1.724	2.968	3.091	3.099	3.143	3.163	6.488	8.255	3.068
1.0	1.635	2.852	3.001	3.016	3.080	3.098	5.826	8.494	3.000
0.8	1.540	3.528	3.269	3.235	3.218	3.248	4.965	7.046	3.105
0.5	2.496	3.999	4.130	4.179	4.196	4.352	4.879	6.269	4.127

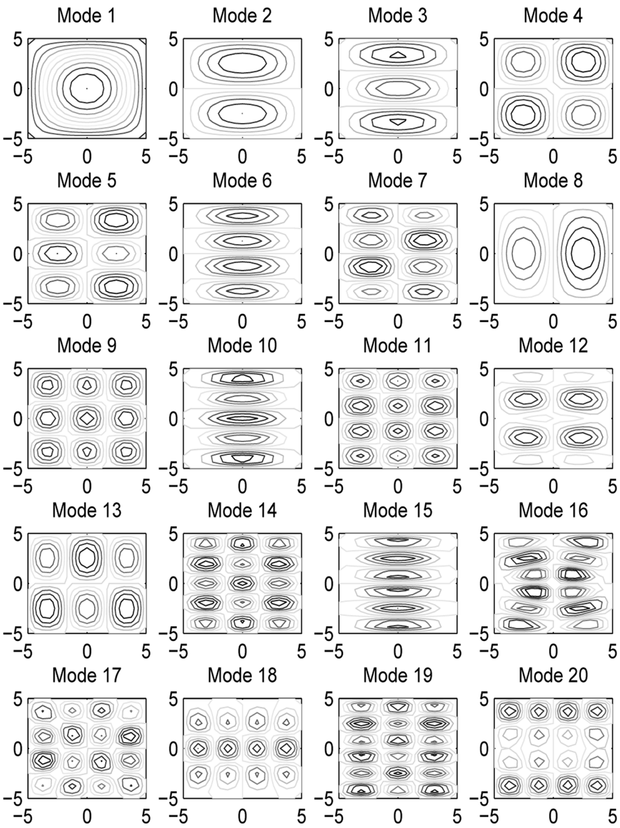

Fig. 5 The first twenty buckling modes of a square orthotropic plate by $D_{22}/D_3 = D_{11}/D_3 = 0.5$

is attempted because the reinforced direction is of great importance with respect to the materials made of orthotropic statement. As desired, both the EFG and present methods give in a remarkable result. The correlation parameter in this buckling analysis might be chosen within a range of $2 \leq \theta \leq 10$ to gain an acceptable solution. The first twenty buckling modes obtained from the present method are also provided in Fig. 5.

3.3 Square plate with a hole of complicated shape

A simply supported thin plate with a hole of complicated shape as shown in Fig. 6 is additionally assessed as the last numerical example. The irregular distributions of 134 and 506 nodes are employed for assessment of static buckling and vibration by both the EFG and the present methods.

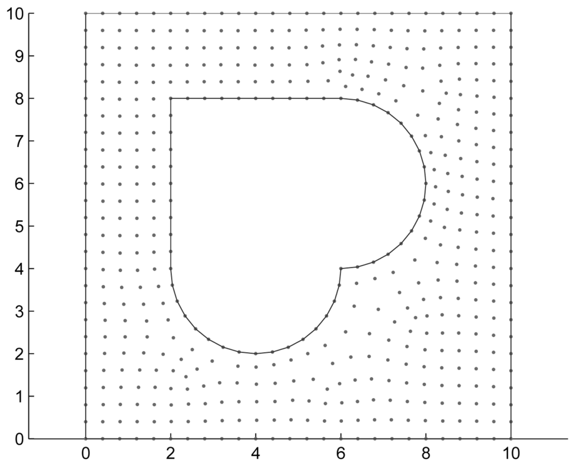

Fig. 6 Geometry and nodal distribution of a plate with a hole of complicated shape

Table 9 Comparison of the dimensionless frequency coefficients for various D_{11}/D_3 of a fully simply supported orthotropic plate with a hole of complicated shape ($\theta = 25$; $\alpha = 2.5$)

Mode	$D_{22}/D_3 = 0.5$					
	$D_{11}/D_3 = 0.5$		$D_{11}/D_3 = 1.0$		$D_{11}/D_3 = 2.0$	
	EFG	Present	EFG	Present	EFG	Present
ξ_1	4.952	4.953	5.026	5.038	5.137	5.160
ξ_2	6.342	6.359	6.465	6.485	6.587	6.554
ξ_3	6.638	6.646	6.861	6.897	7.210	7.221
ξ_4	8.329	8.332	8.575	8.596	8.963	9.037
ξ_5	8.556	8.564	8.879	8.881	9.175	9.207
ξ_6	10.123	10.184	10.332	10.375	10.607	10.674
ξ_7	10.203	10.223	10.844	10.811	11.535	11.569
ξ_8	10.748	10.794	11.365	11.403	12.312	12.355
ξ_9	12.041	12.107	12.532	12.548	13.076	13.134
ξ_{10}	12.286	12.296	12.806	12.832	13.423	13.457

Table 10 Comparison of the critical buckling factor versus various D_{11}/D_3 for a fully simply supported orthotropic plate with a hole of complicated shape ($\theta = 15$; $\alpha = 2.5$)

Approach	Node	$D_{22}/D_3 = 0.5$		
		$D_{11}/D_3 = 0.5$	$D_{11}/D_3 = 1.0$	$D_{11}/D_3 = 2.0$
EFG	134	2.235	2.363	2.567
Present		2.282	2.375	2.588
EFG	506	2.196	2.311	2.490
Present		2.220	2.314	2.506

Other parameters concerning the materials and so on are the same as used the above. Likewise, the dimensionless frequency coefficients and the critical buckling factor are calculated for various flexural rigidity ratios of D_{11}/D_3. The obtained results are presented in Tables 9 and 10, respectively. Excellent agreements to those for both approaches for frequency and critical buckling factors are found as expected.

4. Conclusions

The manuscript reported a successful application of the meshfree moving Kriging interpolation method for vibration and buckling analyses of orthotropic plates. It is evident that by making use of the superior feature of the moving Kriging shape functions, the method is consequently efficient in enforcing the boundary condition. This meshfree formulation in principle permits to account for other problems made of isotropic materials, in which a little modification concerning material properties is required. Through all the achieved results presented above, very good agreements and adequate accuracy compared with other existing approaches are found. A study on the effect of two important parameters on the frequencies and buckling factors is additionally analyzed. The results confirm that, the correlation parameter and the scaling factor may be chosen within wide ranges $2 \leq \theta \leq 10$ and $2.5 \leq \alpha \leq 3.0$ for vibration and buckling problems.

Generally, the present method is very flexible since not only simple rectangular shapes of plates can be solved, but any complicated shapes of geometries are also able to be handled. It is successful in dealing with the buckling and vibration problems of thin orthotropic plates under completely free and fully simply supported boundaries, but the fully clamped one is till open for further developments. The present approach definitely can be considered as an alternative numerical method for free vibration and buckling analysis of orthotropic plates with high accuracy. As a consequence, it is absolutely promising and potential for other applications, especially in fracture mechanics where enrichment techniques (Fleming *et al.* 1997) can be incorporated, nonlinear analysis and so on.

References

Allman, D.J. (1975), “Calculation of the elastic buckling loads of thin flat reinforced plates using triangular finite elements”, *Int. J. Numer. Meth. Eng.,* **9**, 415-432.

Ahmadian, M.T. and Sherafati Zangened, M. (2002), "Vibration analysis of orthotropic rectangular plates using superelements", *Comput. Meth. Appl. Mech. Eng.,* **191**, 2069-2075.

Atluri, S.N. and Zhu, T. (1998), "A new meshless local Petrov-Galerkin (MLPG) approach in computational mechanics", *Comput. Mech.,* **22**, 117-127.

Bank, C.L. and Yin, J. (1996), "Buckling of orthotropic plates with free and rotationally restrained unloaded edges", *Thin Wall. Struct.,* **24**, 83-96.

Batra, R.C., Qian, L.F. and Chen, L.M. (2004), "Natural frequencies of thick square plates made of orthotropic, trigonal, monoclinic and triclinic materials", *J. Sound Vib.,* **270**, 1074-1086.

Belytschko, T., Lu, Y.Y. and Gu, L. (1994), "Element free Galerkin method", *Int. J. Numer. Meth. Eng.,* **37**, 229-256.

Belyschko, T., Organ, D. and Krongauz, Y. (1995), "A coupled finite element-element frer Galerkin method", *Comput. Mech.,* **17**, 186-195.

Biancolini, M.E., Brutti, C. and Reccia, L. (2005), "Approximate solution for free vibrations of thin orthotropic rectangular plates", *J. Sound Vib.,* **288**, 321-344.

Bui, Q.T., Nguyen, N.T. and Nguyen-Dang, H. (2009), "A moving Kriging interpolation-based meshless method for numerical simulation of Kirchhoff plate problems", *Int. J. Numer. Meth. Eng.,* **77**, 1371-1395.

Bui, Q.T., Nguyen, N.M. and Zhang, Ch. (2010), "A moving Kriging interpolation-based element-free Galerkin method for structural dynamic analysis", *Comput. Meth. Appl. Mech. Eng.* **200**, 1354-1366.

Bui, Q.T., Nguyen, N.M., Zhang, Ch. and Pham, D.A.K. (2011), "An efficient meshfree method for analysis of two-dimensional piezoelectric structures", *Smart Mater. Struct.,* **20**, 065016.

Chen, J.S., Wu, C.T., Yoon, S. and You, Y. (2001), "A stabilized conforming nodal integration for Galerkin mesh-free methods", *Int. J. Numer. Meth. Eng.,* **50**, 435-466.

Chen, X.L., Liu, G.R. and Lim, S.P. (2003), "An element free Galerkin method for the free vibration analysis of composite laminates of complicated shape", *Compos. Struct.,* **59**, 279-289.

Chen, Y.Z. (1998), "Evaluation of fundamental vibration frequency of an orthotropic bending plate by using an iterative approach", *Comput. Meth. Appl. Mech. Eng.,* **161**, 289-296.

Cui, X.Y., Liu, R.G. and Li, G. (2009), "A smoothed Hermite radial point interpolation method for thin plate analysis", *Arch. Appl. Mech.,* **81**(1), 1-18.

Cui, X.Y., Liu, G.R., Li, G.Y. and Zhang, G.Y. (2011), "A thin plate formulation without rotation DOFs based on the radial point interpolation method and triangular cells", *Int. J. Numer. Meth. Eng.,* **85**(8), 958-986.

Ferreira, A.J.M. and Batra, R.C. (2005), "Natural frequencies of orthotropic, monoclinic and hexagonal plates by a meshless method", *J. Sound Vib.,* **285**, 734-742.

Ferreura, A.J.M., Fasshauer, G.E. and Batra, R.C. (2009), "Natural frequencies of thick plates made of orthotropic, monoclinic and hexagonal plates by a meshless method", *J. Sound Vib.,* **319**, 984-992.

Fleming, M., Chu, Y.A., Moran, B. and Belyschko, T. (1997), "Enriched element-free Galerkin methods for crack tip fields", *Int. J. Numer. Meth. Eng.,* **40**, 1483-1504.

Gu, L. (2003), "Moving Kriging interpolation and element free Galerkin method", *Int. J. Numer. Meth. Eng.,* **56**, 1-11.

James, O. (2010), "Comparing finite element and meshfree particle formulations for projectile penetration into fiber reinforced concrete", *Comput. Concrete*, **7**(1), 103-110.

Jones, M.R. (2006), *Buckling of Bars, Plates, and Shells,* Bull Ridge Publishing, Blacksburg, Virginia, USA.

Krysl, P. and Belytschko, T. (1996), "Analysis of thin plate by the element free Galerkin method", *Comput. Mech.,* **17**, 26-35.

Leissa, W.A. (1977), "Recent research in plate vibrations: complicating effects", *Shock Vib.,* **9**, 21-35.

Leissa, W.A. (1981), "Plate vibration research 1976-1981: complicating effects", *Shock Vib.,* **13**, 19-36.

Leissa, W.A. (1987), "Recent research in plate vibrations. 1981-1985-Part II: complicating effects", *Shock Vib.,* **19**, 10-24.

Li, S. and Liu, W.K. (2004), *Meshfree Particle Method*, Springer Berlin-Heidelberg, New York.

Liew, K.M. and Chen, X.L. (2004), "Mesh-free radial point interpolation method for the buckling analysis of Mindlin plates subjected to in-plane point loads", *Int. J. Numer. Meth. Eng.,* **60**, 1861-1877.

Liew, K.M., Zhao, X. and Ferreira, A.J.M. (2011), "A review of meshfree methods for laminated and functionally graded plates and shells", *Compos. Struct.,* **93**, 2031-2041.

Liew, K.M., Xiang, Y. and Kitipornchai, S. (1995), "Research on thick plate vibration-A literature survey", *J. Sound Vib.,* **180**, 163-176.
Liu, W.K., Jun, S. and Zhang, Y.F. (1996), "Reproducing kernel particle method", *Int. J. Numer. Meth. Fluids,* **20**, 1081-1106.
Liu, G.R. and Gu, Y.T. (2001), "A point interpolation method for two-dimensional solids", *Int. J. Numer. Meth. Eng.,* **50**, 937-951.
Liu, G.R. (2003), *Meshfree Methods, Moving Beyond the Finite Element Method*, CRC Press, USA.
Liu, G.R. and Chen, X.L. (2001), "A mesh-free method for static and free vibration analyses of thin plates of complicated shape", *J. Sound Vib.,* **241**, 839-855.
Liu, Y., Hon, Y.X. and Liew, K.M. (2006), "A meshfree Hermite-type radial point interpolation method for Kirchhoff plate problems", *Int. J. Numer. Meth. Eng.,* **66**, 1153-1178.
Lok, T.S. and Cheng, Q.H. (2001), "Free and forced vibration of simply supported, orthotropic sandwich panel", *Comput. Struct.,* **79**, 301-312.
Matsubara, H. and Yagawa, G. (2009), "Convergence studies for enriched free mesh method and its application to fracture mechanics", *Interact. Multi. Mech.,* **2**, 277-293.
Sadeghirad, A., Mohammadi, S. and Kani, I.M. (2010), "Meshless equilibrium on line method (MELM) for linear elasticity", *Struct. Eng. Mech.,* **35**(4), 511-533.
Sayakoummane, V. and Kanok-Nukulchai, W. (2007), "A meshless analysis of shells based on moving Kriging interpolation", *Int. J. Comput. Meth.,* **4**, 543-565.
Singh, A., Singh, I.V. and Prakash, R. (2007), "Meshless element free Galerkin method for unsteady nonlinear heat transfer problems", *Int. J. Heat Mass Trans.,* **50**, 1212-1219.
Tongsuk, P. and Kanok-Nukulchai, W. (2004), "Further investigation of element free Galerkin method using moving Kriging interpolation", *Int. J. Comput. Meth.,* **1**, 345-365.
Wang, D. and Wu, Y. (2008), "An efficient Galerkin meshfree analysis of shear deformable cylindrical panels", *Interac. Multisc. Mech.,* **1**, 339-355.
Wang, S. (1997), "A unified Timoshenko beam B-spline Rayleigh-Ritz method for vibration and buckling analysis of think and thin beams and plates", *Int. J. Numer. Meth. Eng.,* **40**, 473-491.
Wanji, C. and Cheung, Y.K. (1998), "Refined triangular discrete Kirchhoff plate element for thin plate bending, vibration and buckling analysis", *Int. J. Numer. Meth. Eng.,* **41**, 1507-1525.
Vinson, R.J. (2005), *Plate and Panel Structures of Isotropic, Composite and Piezoelectric Materials, Including Sandwich Construction*, Springer, USA.
Zienkiewicz, O.C. and Taylor, R.L. (1989), *The Finite Element Method*, McGraw-Hill, New York.

Notations

x, y, z	: axis of the reference system
u, v, w	: displacement components belong to x, y, z
E_1	: Young's modulus in bending for the x-direction
E_2	: Young's modulus in bending for the y-direction
G_{12}	: Shear modulus in bending for the xy plane
ν_{12}	: Poisson's ratio corresponding to compression strain in y-direction
ν_{21}	: Poisson's ratio corresponding to compression strain in x-sdirection
ρ	: the mass density of the material
h	: thickness of the plate
a	: length of side parallel to x-axis
b	: length of side parallel to y-axis
θ	: correlation parameter
α	: scaling factor
w	: transverse displacement of a point on the plate along z-direction
ϕ	: meshfree MK shape function
$\mathbf{N}$	: components of in-plane forces acting on the plate on its edges
M_x, M_y and M_{xy}	: bending and twisting moments
$\mathbf{D}$	: matrix of material constants
ω	: circular frequency
t	: time
N_0	: critical buckling loads
ξ	: dimensionless natural frequency coefficient
k	: critical buckling factor